

## Electronic Supplementary Information

### **Enhanced Electrical Properties of Microcellular Polymer Nanocomposites via Nanocarbon Geometrical Alteration: A Comparison of Graphene Nanoribbon and its Parent Multiwalled Carbon Nanotube**

*Meysam Salari, Saeed Habibpour, Mahdi Hamidinejad, \* Sara Mohseni Taromsari, Hani E. Naguib, Aiping Yu, Chul B. Park\**

M. Salari, S. M. Taromsari, H. E. Naguib, C. B. Park  
Department of Mechanical and Industrial Engineering, University of Toronto, 5 King's College Road, Toronto, M5S 3G8, Canada  
Corresponding Authors' Emails: [mahdi.hamidi@ualberta.ca](mailto:mahdi.hamidi@ualberta.ca), [park@mie.utoronto.ca](mailto:park@mie.utoronto.ca)

S. Habibour, A. Yu  
Department of Chemical Engineering, University of Waterloo, 200 University Avenue West, Waterloo, N2L 3G1, Canada

M. Hamidinejad  
Department of Mechanical Engineering, University of Alberta, 9211-116 Street NW, Edmonton, AB T6G1H9, Canada

## **S1. Nanofillers Synthesis and Characterizations**

### **S1.1. Nanofillers Synthesis**

In this work, graphene nanoribbon (GNR) was produced via improved Hummer's method [S1]. Accordingly, the process involves oxidative unzipping of multiwalled carbon nanotube (MWCNT) to synthesize graphene oxide nanoribbon (GONR), followed by a thermal reduction to remove the oxygen-containing groups. The details of the experimental steps are as follows: (1) 1 g MWCNT was dispersed in an acidic mixture of 180 ml sulfuric acid and 20 ml phosphoric acid and stirred for 1 hr at 0 °C (ice bath). (2) 5 g potassium permanganate (that is the oxidizing agent) was added to the reactor gradually in 30 min. During the next 1 hr, the temperature of the mixture was increased from room temperature to 65 °C at which it stirred for 3 additional hours. (3) The mixture was cooled to the room temperature and poured to 200 ml ice bath containing 10 ml hydrogen peroxide. The solution containing GONR was allowed to precipitate for 24 hrs, then the slurry was poured to the dialysis tube until pH reached 6–7. The solution was subsequently freeze-dried to obtain GONR powder. (4) Finally, in order to remove the functional groups of GONR, a thermal reduction under an argon atmosphere was conducted using an alumina ceramic boat according to the following temperature profile: heating by a rate of 3 °C/min from the room temperature to 550 °C, directly followed by heating by a rate of 10 °C/min from 550 °C to 900 °C, then cooling down to the room temperature.

### **S1.2. Nanofillers Characterizations**

The intrinsic conductivities of the nanofillers govern the CPCs' electrical conductivities. Hence,  $\sigma_{DC}$  of the compressed powders of the parent MWCNT and GNR were measured. According to Figure S1A, compressed MWCNT with  $\sigma_{DC} \approx 4.36$  S/cm shows around 18 times superior

conductivity than GNR with  $\sigma_{DC} \approx 0.24$  S/cm. The MWCNT's greater electrical conductivity can be attributed to two main reasons: (I) the charge redistribution induced by its curved geometry causing a build-in electrostatic field perpendicular to the surface [S2,S3]; and (II) the structural defects which formed due to the oxidation and did not restore after the reduction process during the nanotube-to-nanoribbon conversion [S4,S5].

Figure S1B shows the nitrogen adsorption and desorption isotherms of the parent MWCNT and GNR. The calculated specific surface areas of the nanofillers by Brunauer-Emmett-Teller (BET) analysis reveal a 142% surface area improvement by unzipping process. As shown, GNR possesses a surface area of 382.6 m<sup>2</sup>/g while MWCNT have a surface area of 158.2 m<sup>2</sup>/g.

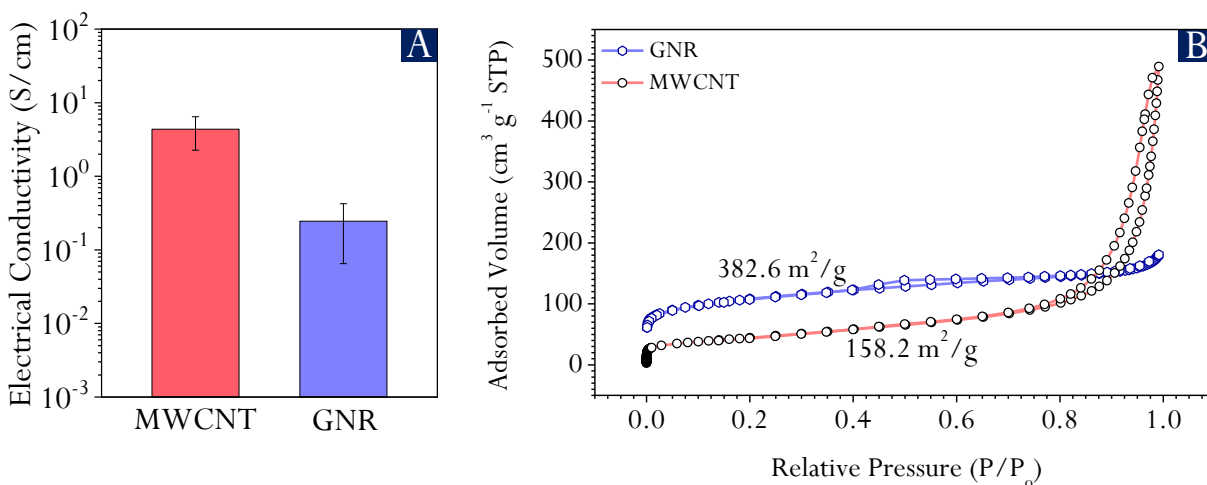


**Figure S1.** (A) Electrical conductivity of the compressed powders of the parent MWCNT and GNR. (B) The nitrogen adsorption and desorption isotherms and the calculated specific surface areas of the nanofillers.

Table S1 compares Electrical conductivity of GNRs synthesized from CNT through different methods. As shown, the range of the electrical conductivity values is highly related to the measurement method and sample preparation. However, in all cases, the electrical conductivity of the produced GNR is significantly related to conductivity of the parent CNT used for its synthesis.

**Table S1.** Electrical conductivity of GNRs synthesized from CNT through different methods.

Synthesis Method	Conductivity Measurement System (Sample Type)	Electrical Conductivity (S/m)		Refs.
		Parent CNT	GNR	
Na/K Alloy Intercalation	4-Point Probe System (Compressed Powder)	~10	4 – 40	[S6,S7]
Na/K Alloy Intercalation	4-Point Probe System (High Pressure Pressed Pellet)	32,000 – 61,500	10,500 – 23,500	[S8]
		13,500 – 72,000	13,000 – 15,500	
Electrochemical Unzipping	2-Point Probe System (Drop Casted Dispersed Powder)	~20,600	~24,500	[S9]
Oxidative Unzipping	Probe Station System (Deposited GNRs onto Si/SiO <sub>2</sub> Substrates)	N/A	~4,000	[S10]
Potassium Vapour Splitting	Probe Station System (Deposited GNRs onto Si/SiO <sub>2</sub> Substrates)	N/A	~80,000	[S11]
Oxidative Unzipping	4-Point Probe System (Compressed Powder)	~436	~24	This Work

The optical bandgap ( $E_{opt}$ ) of the nanofillers were measured through the Tauc method [S12,S13].

Accordingly, the absorption coefficient ( $\alpha$ ) and the photon energy, i.e.,  $h\nu$  ( $h = 4.1357$  eV·s:

Planck's constant,  $\nu = \frac{2.998 \times 10^8 \text{ m/s}}{\lambda}$ : photon's frequency;  $\lambda$  is the wavelength) in many semiconductors show the following empirical relation:

$$(\alpha h\nu)^\gamma = A(h\nu - E_{opt}) \quad (S1)$$

where  $A$  is a proportionality constant which, in UV-Vis spectroscopy, is equal to the absorbance as a dimensionless quantity;  $\gamma$  indicates the nature of the electronic transition, so that  $\gamma = \frac{1}{2}$  and 2 denote indirect and direct allowed transitions, respectively. Based on Beer–Lambert law, the absorption coefficient and absorbance can be related as  $\alpha = 2.302 A \text{ cm}^{-1}$ . As shown in Figure S2A and S2B, the direct  $E_{opt}$  of the nanofillers are estimated by the extrapolation of the linear regions of their corresponding Tauc plots.

The measured  $E_{opt}$  confirm the comparatively more facile charge transport in MWCNT with  $E_{opt} = 3.58$  eV which is approximately 0.4 eV less than that of GNR with  $E_{opt} = 3.97$  eV. It is worth mentioning that in some semiconductors, including the nanofillers used in this study, the

distinction between the optical bandgap and the electronic bandgap ( $E_g$ ), which is the energy difference between the valence band and the conduction band, cannot be ignored. However,  $E_{opt}$  can be still approximated as  $E_g$ , especially in such comparative studies [S12].

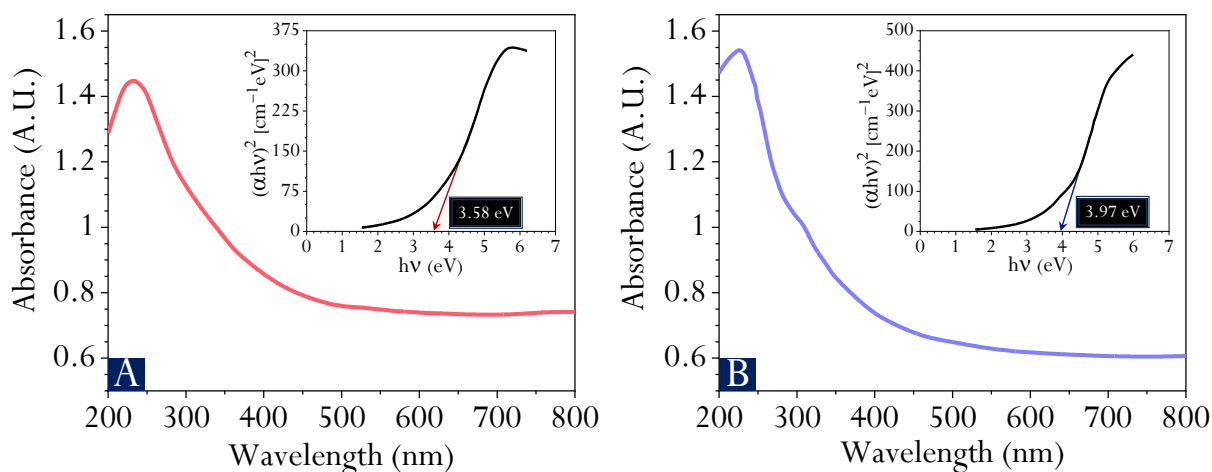


**Figure S2.** UV-Vis spectra and Tauc plots for (A) the parent MWCNT, and (B) GNR.

## S2. Nanocomposites Characterizations

### S2.1. Solid Nanocomposites Characterization

According to Figure S3A, the nanocomposites containing 0.2 – 1.7 vol% show relatively close conductivity values at the insulative region where an almost linear increase is observed. This is attributed to lack of effective contacts between isolated nanofillers within the polymeric medium. In Figure S3B, Raman spectra (in the Raman shift of 600–1000 cm<sup>-1</sup>) of the nanocomposites containing 2.5 vol% CNT and GNR are shown. The peaks at 612 and 804 cm<sup>-1</sup> signify  $\alpha$ -PVDF, which are assigned to backbone deformation modes involving CCF + CCC and CC + CCC, respectively [S14,S15]. The  $\beta$ -PVDF is characterized by the peak at 842 cm<sup>-1</sup> corresponding to CF stretching mode. According to the relatively intensified peak assigned to  $\beta$ -PVDF in the CNT case,

it can be observed that CNT induces a more pronounced nucleating effect for the  $\beta$ -phase formation, compared to GNR. This implies that CNT would show a relatively stronger interfacial interaction, providing the fluorine matrix with a substrate onto which the polymer backbone with different chain conformations can be attached [S6,S16]. As mentioned in Introduction, a curvature-induced rehybridization between  $\pi$  and  $\sigma$  orbitals takes place in CNT, which changes the degree of hybridization from  $sp^2$  to  $sp^{2+\eta}$ , where  $\eta$  is a fractional number  $0 < \eta < 1$ , (i.e., an intermediate state between  $sp^2$  and  $sp^3$ ). This leaves a free hybrid orbital available for stronger interaction with the matrix [S3,S6].

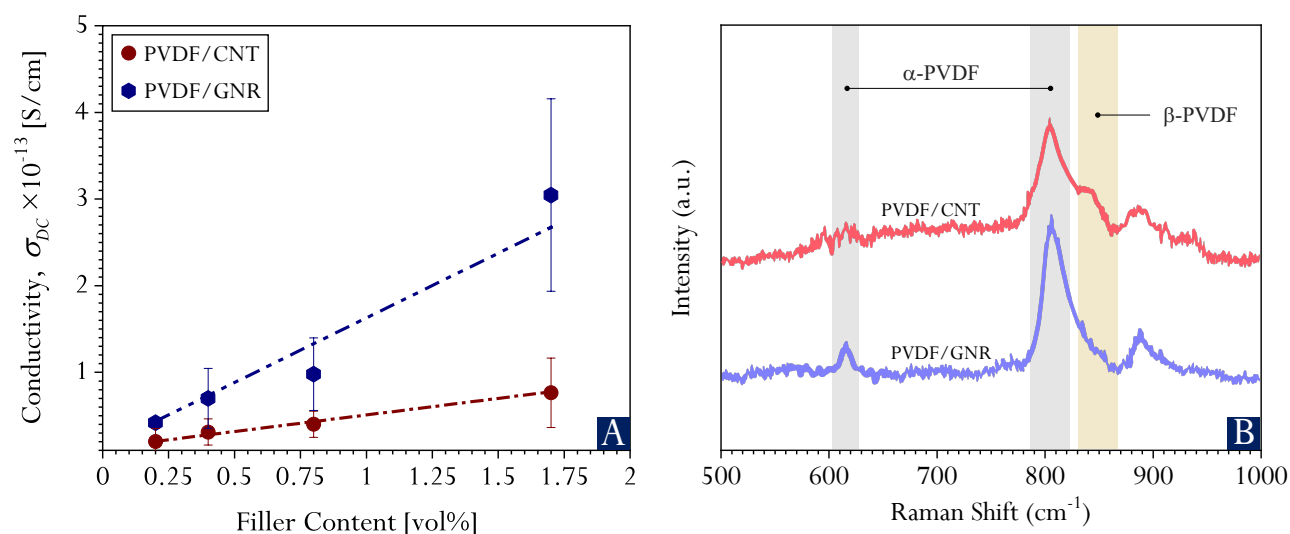


**Figure S3.** (A) DC electrical conductivity of the nanocomposites (measured at  $1 \times 10^{-1}$  Hz) in the insulative region. (B) Raman spectra of MWCNT and GNR nanocomposites (2.5 vol%).

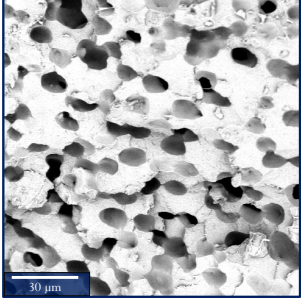
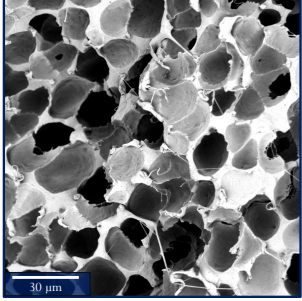
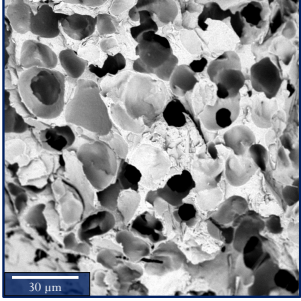
## S2.2. Microcellular Nanocomposites Characterizations

The relative densities of the composites ( $\rho_{rel} = \frac{\rho_f}{\rho_s}$ ;  $\rho_s$  and  $\rho_f$  are the densities of the samples before and after foaming, respectively) were measured using the water displacement method according to ASTM-D792. Then, the composites' volume expansion ratios ( $\Phi$ ) and their void fractions ( $v_f$ ) were calculated by means of the following expressions:

$$\Phi = \frac{1}{\rho_{rel}} \quad (S2)$$

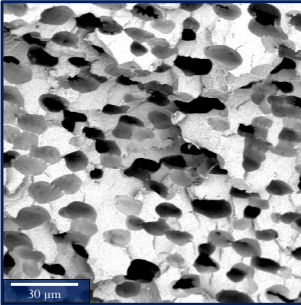
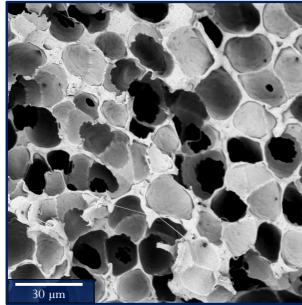
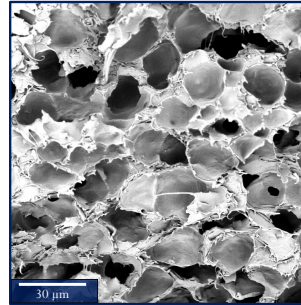
$$v_f = 1 - \frac{1}{\Phi} = 1 - \rho_{rel} \quad (S3)$$

**Table S2.** Microcellular structure parameters and the SEM images of the PVDF/4.2 vol% CNT composites.

Sample	F-CNT1	F-CNT2	F-CNT3
Temperature (°C)	165.5	168	170.5
$\Phi$	$2.0 \pm 0.16$	$3.2 \pm 0.48$	$2.1 \pm 0.14$
$v_f (v_{f_2}^*)$	$49.3 \pm 4.3 (26.3 \pm 3.6)$	$68.8 \pm 4.7 (37.9 \pm 4.8)$	$51.5 \pm 3.5 (27.1 \pm 5.1)$
SEM			

\*  $v_{f_2}$  denotes the void fractions of the foamed samples after the post-compression molding at 125°C.

**Table S3.** Microcellular structure parameters and the SEM images of the PVDF/4.2 vol% GNR composites.

Sample	F-GNR1	F-GNR2	F-GNR3
Temperature (°C)	165.5	168	170.5
$\Phi$	$2.1 \pm 0.21$	$3.6 \pm 0.68$	$2.2 \pm 0.13$
$v_f (v_{f_2}^*)$	$50.7 \pm 4.8 (26.8 \pm 3.3)$	$72.4 \pm 5.2 (41.3 \pm 4.1)$	$54.1 \pm 2.9 (28.4 \pm 4.3)$
SEM			

\*  $v_{f_2}$  denotes the void fractions of the foamed samples after the post-compression molding at 125°C.

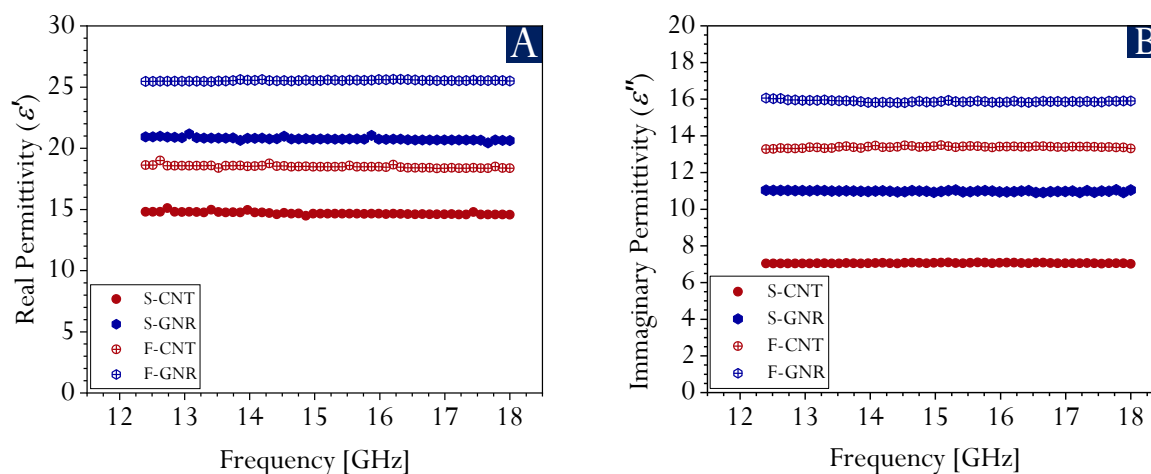


**Figure S4.**  $K_u$ -band (A) real and (B) imaginary dielectric permittivity of the solid and microcellular nanocomposites with 4.2 vol% nanofiller.

## References

- [S1] D. V Kosynkin, A.L. Higginbotham, A. Sinitskii, J.R. Lomeda, A. Dimiev, B.K. Price, J.M. Tour, Longitudinal unzipping of carbon nanotubes to form graphene nanoribbons, *Nature*. 458 (2009) 872–876.
- [S2] T. Dumitrică, C.M. Landis, B.I. Yakobson, Curvature-induced polarization in carbon nanoshells, *Chem. Phys. Lett.* 360 (2002) 182–188.
- [S3] O. Yu, P. Jing-Cui, W. Hui, P. Zhi-Hua, The rehybridization of electronic orbitals in carbon nanotubes, *Chinese Phys. B.* 17 (2008) 3123.
- [S4] N. Gorjizadeh, A.A. Farajian, Y. Kawazoe, The effects of defects on the conductance of graphene nanoribbons, *Nanotechnology*. 20 (2008) 15201.
- [S5] Y. Jun, S. Habibpour, M. Hamidinejad, M.G. Park, W. Ahn, A. Yu, C.B. Park, Enhanced electrical and mechanical properties of graphene nano-ribbon/thermoplastic polyurethane composites, *Carbon N. Y.* 174 (2021) 305–316.
- [S6] S. Sadeghi, M. Arjmand, I. Otero Navas, A. Zehtab Yazdi, U. Sundararaj, Effect of nanofiller geometry on network formation in polymeric nanocomposites: Comparison of rheological and electrical properties of multiwalled carbon nanotube and graphene nanoribbon, *Macromolecules*. 50 (2017) 3954–3967.
- [S7] M. Arjmand, S. Sadeghi, M. Khajepour, U. Sundararaj, Carbon Nanotube/Graphene Nanoribbon/Polyvinylidene Fluoride Hybrid Nanocomposites: Rheological and Dielectric Properties, *J. Phys. Chem. C.* 121 (2017) 169–181. <https://doi.org/10.1021/acs.jpcc.6b10741>.
- [S8] B. Genorio, W. Lu, A.M. Dimiev, Y. Zhu, A.-R.O. Raji, B. Novosel, L.B. Alemany, J.M. Tour, In situ intercalation replacement and selective functionalization of graphene nanoribbon stacks, *ACS Nano*. 6 (2012) 4231–4240.
- [S9] D.B. Shinde, J. Debgupta, A. Kushwaha, M. Aslam, V.K. Pillai, Electrochemical unzipping of multi-walled carbon nanotubes for facile synthesis of high-quality graphene nanoribbons,

- J. Am. Chem. Soc. 133 (2011) 4168–4171.
- [S10] A.L. Higginbotham, D. V Kosynkin, A. Sinitskii, Z. Sun, J.M. Tour, Lower-defect graphene oxide nanoribbons from multiwalled carbon nanotubes, *ACS Nano*. 4 (2010) 2059–2069.
- [S11] D. V Kosynkin, W. Lu, A. Sinitskii, G. Pera, Z. Sun, J.M. Tour, Highly conductive graphene nanoribbons by longitudinal splitting of carbon nanotubes using potassium vapor, *ACS Nano*. 5 (2011) 968–974.
- [S12] Z. Chen, T. Jaramillo, The Use of UV-Visible Spectroscopy to Measure the Band Gap of a Semiconductor, (2017).
- [S13] P. Makuła, M. Pacia, W. Macyk, How to correctly determine the band gap energy of modified semiconductor photocatalysts based on UV–Vis spectra, *J. Phys. Chem. Lett.* 9 (2018) 6814–6817.
- [S14] Y. Yang, G. Wu, S. Ramalingam, S.L. Hsu, L. Kleiner, F.W. Tang, Spectroscopic analysis of amorphous structure in fluorinated polymers, *Macromolecules*. 40 (2007) 9658–9663.
- [S15] P. Viswanath, M. Yoshimura, Light-induced reversible phase transition in polyvinylidene fluoride-based nanocomposites, *SN Appl. Sci.* 1 (2019) 1–9. <https://doi.org/10.1007/s42452-019-1564-3>.
- [S16] M. Arjmand, S. Sadeghi, I. Otero Navas, Y. Zamani Keteklahijani, S. Dordanihaghighi, U. Sundararaj, Carbon nanotube versus graphene nanoribbon: impact of nanofiller geometry on electromagnetic interference shielding of polyvinylidene fluoride nanocomposites, *Polymers (Basel)*. 11 (2019) 1064.